Synthesis of Porous Single Crystals of Metal Oxides via a Solid−Liquid Route

Wenbo Yue and Wuzong Zhou*

School of Chemistry, University of St. Andrews, St. Andrews, Fife KY16 9ST, United Kingdom

Received January 14, 2007. Revised Manuscript Received February 18, 2007

Porous single crystals of Co_3O_4, NiO, CeO_2, and Cr_2O_3 were produced using mesoporous silicas, SBA-15 and KIT-6, as hard templates and a new convenient approach, the solid−liquid method, was developed. Characterization of the materials was performed mainly by using X-ray powder diffraction and high-resolution transmission electron microscopy. The advantages and disadvantages of this solvent-free method are discussed in comparison with the previously established methods.

1. Introduction

Since the first ordered mesoporous silica MCM-41[1] was reported by Mobil scientists using self-assembled organic surfactants as soft templates in the 1990s, many new types of mesoporous silicas, including SBA-15[2,3] and KIT-6,[4] have been synthesized. In addition to many possible applications, the space of the regular channels in these materials have been used as nanoreactors for producing mesoporous composites[5,6] and as hard templates for crystal growth of porous metal oxides.[7−13] For example, porous crystals of Cr_2O_3,[7,10,11] Co_3O_4,[8,9,11,12] and NiO[8,9,13] were produced by using mesoporous SBA-15 and KIT-6 silicas as hard templates. These mesoporous metal oxides have potential application in various industries, used as new materials for gas sensors,[14,15] the precursor of anode materials in Li-ion rechargeable batteries,[14,16] and catalysts[17−19] because of their large specific surface areas and shape-selective properties, which enhances the efficiency of catalysis, conduction, and adsorption.

The general route for producing the porous crystals of oxides using mesoporous silica as template is introducing a metal-containing precursor into the silica pores, allowing the precursor to decompose followed by crystal growth of metal oxides inside the pores during thermal treatment. Therefore, a crucial step in the above process is the impregnation of the precursor. Three methods of impregnation have been previously developed, the so-called surface modification method, "two solvents" method, and evaporation method, respectively. In the surface modification method, the inner surface of the mesoporous silica template is functionalized via aminosilylation of the surface silanols and then a selected heteropolyacidic precursor (e.g., $H_2Cr_2O_7$ for Cr_2O_3 and $H_3PW_{12}O_{40}$ for WO_3) is anchored.[7,20,21] The functionalized surface is positively charged and the metal-containing ions are negatively charged (heteropolyacidic anions). Therefore, the driving force of migration of the precursor is mainly ionic attraction. In the "two solvents" impregnation method, a suspension of mesoporous silica in dry hexane is mixed with an aqueous solution of metal nitrate. The precursor molecules will then move into the pores during overnight stirring.[10] In the evaporation method, the mesoporous silica template is mixed with metal nitrate in ethanol. It was expected that the precursor nitrate would enter the pores during the evaporation of ethanol by a capillary action.[8,9,11] In addition, if a metal-containing precursor is reactive with silica, mesoporous carbon,[22,23] which is fabricated using mesoporous silica as a template, can be used as a hard template for preparing the

* To whom correspondence should be addressed. E-mail: wzhou@st-andrews.ac.uk. Tel.: +44 1334 467276. Fax: +44 1334 463808.

(1) Kresge, C. T.; Leonowicz, M. E.; Roth, J.; Vartuli, J. C.; Beck, J. S. *Nature* **1992**, *359*, 710.
(2) Zhao, D. Y.; Feng, J. L.; Huo, Q. S.; Melosh, N.; Fredrickson, G. H.; Chmelka, B. F.; Stucky, G. D. *Science* **1998**, *279*, 548.
(3) Zhao, D. Y.; Huo, Q. S.; Feng, J. L.; Chmelka, B. F.; Stucky, G. D. *J. Am. Chem. Soc.* **1998**, *120*, 6024.
(4) Kleitz, F. Choi, S. H.; Ryoo, R. *Chem. Commun.* **2003**, 2136.
(5) Lu, A. H.; Schmidt, W.; Kiefer, W.; Schüth, F. *J. Mater. Sci.* **2005**, *40*, 5091.
(6) Fan, J.; Shui, W. Q.; Yang, P. Y.; Wang, X. Y.; Xu, Y. M.; Wang, H. H.; Chen, X.; Zhao, D. Y. *Chem. Eur. J.* **2005**, *11*, 5391.
(7) Zhu, K. K.; Yue, B.; Zhou, W. Z.; He, H. Y. *Chem. Commun.* **2003**, 98.
(8) Tian, B. Z.; Liu, X. Y.; Yang, H. F.; Xie, S. H.; Yu, C. Z.; Tu, B.; Zhao, D. Y. *Adv. Mater.* **2003**, *15*, 1370.
(9) Tian, B. Z.; Liu, X. Y.; Solovyov, L. A.; Liu, Z.; Yang, H. F.; Zhang, Z. D.; Xie, S. H.; Zhang, F. Q.; Tu, B.; Yu, C. Z.; Terasaki, O.; Zhao, D. Y. *J. Am. Chem. Soc.* **2004**, *126*, 865.
(10) Jiao, K.; Zhang, B.; Yue, B.; Ren, Y.; Liu, S. X.; Yan, S. R.; Dickinson, C.; Zhou, W. Z.; He, H. Y. *Chem. Commun.* **2005**, 5618.
(11) Dickinson, C.; Zhou, W. Z.; Hodgkins, R. P.; Shi, Y. F.; Zhao, D. Y.; He, H. Y. *Chem. Mater.* **2006**, *18*, 3088.
(12) Wang, Y. Q.; Yang, C. M.; Schmidt, W.; Spliethoff, B.; Bill, E.; Schuth, F. *Adv. Mater.* **2005**, *17*, 53.
(13) Wang, Y. G.; Xia, Y. Y. *Electrochim. Acta* **2006**, *51*, 3223.
(14) Li, W. Y.; Xu, L. N.; Chen, J. *Adv. Funct. Mater.* **2005**, *15*, 851.
(15) Hotovy, I.; Rehacek, V.; Siciliano, P.; Capone, S.; Spiess, L. *Thin Solid Films* **2002**, *418*, 9.
(16) Jiao, F.; Shaju, K. M.; Bruce, P. G. *Angew. Chem., Int. Ed.* **2005**, *44*, 6550.
(17) Yan, L.; Zhang, X. M.; Ren, T.; Zhang, H. P.; Wang, X. L.; Suo, J. S. *Chem. Commun.* **2002**, 860.
(18) Moreno-Tost, R.; Santamaria-Gonzalez, J.; Maireles-Torres, P.; Rodriguez-Castellon, E.; Jimenez-Lopez, A. *J. Mater. Chem.* **2002**, *12*, 3331.
(19) Miao, J. W.; Zhou, J.; Song, G. H.; Fan, Y. N.; Gong, C. *Chin. J. Inorg. Chem.* **2005**, *21*, 1541.
(20) Yue, B.; Tang, H. L.; Kong, Z. P.; Zhu, K. K.; Dickinson, C.; Zhou, W. Z.; He, H. Y. *Chem. Phys. Lett.* **2005**, *407*, 83.
(21) Kaleta, W.; Nowinska, K. *Chem. Commun.* **2001**, 535.
(22) Shin, H. J.; Ryoo, R.; Kruk, M.; Jaroniec, M. *Chem. Commun.* **2001**, 349.
(23) Ryoo, R.; Joo, S.; Kruk, M.; Jaroniec, M. *Adv. Mater.* **2001**, *13*, 677.

10.1021/cm070124b CCC: $37.00 © 2007 American Chemical Society
Published on Web 03/20/2007

porous metal oxides.[24−26] In this case, the final product is a positive replica of the mesoporous silica. Mesoporous carbon was also successfully used as a template for producing mesoporous zeolite crystals.[27]

During the course of our studies of crystal growth in mesopores, we noticed that metal-containing precursors can also be introduced into the mesopores simply by grinding a mixed powder of the precursor and a silica template. This phenomenon was also observed by other groups.[28−30] However, the mechanism is yet to be fully understood. In the present work, we demonstrate this new synthesis method, designated the solid−liquid method because the precursor must be melted at an early stage, in preparation of porous single crystals of Co_3O_4, NiO, CeO_2, and Cr_2O_3, using SBA-15 and KIT-6 as hard templates.

2. Experimental Section

Mesoporous silicas SBA-15 and KIT-6 were synthesized according to the corresponding literature[2−4] and the surfactants were removed by heating the as-synthesized specimens at 550 °C for 5 h. One millimole of precursor $X_m(NO_3)_n{\cdot}yH_2O$ (X = Co, Ni, Ce, or Cr) was mixed with 0.15 g of mesoporous silica and was ground for a few minutes in an agate mortar and pestle. The mix was then put into a crucible, which was placed in a muffle furnace. The temperature was increased from room temperature to 500 °C at a rate of 1 °C/min and maintained at the final temperature for 5 h. The specimen was then cooled down to room temperature. The silica template was removed by a 10 wt % HF aqueous solution (for Co_3O_4, Cr_2O_3) or 2 M hot NaOH solution (80 °C, for NiO, CeO_2). For the HF treatment, the metal oxide containing mesoporous silica was placed in a polyethylene bottle with 10% HF, and the solution was stirred overnight. The same procedure was used in the NaOH treatment with replacement of HF by NaOH and keeping the solution warm. The porous metal-oxide products were recovered by centrifugation and washed with distilled water three times.

To investigate the mechanisms of impregnation and decomposition of the precursor, and the crystal growth of metal oxides, a series of Cr-containing specimens templated by SBA-15 were collected at different stages of the thermal treatment, e.g., at 70 °C (a little higher than the melting point of $Cr(NO_3)_3{\cdot}9H_2O$), 110 °C (just above the decomposition temperature of $Cr(NO_3)_3{\cdot}9H_2O$), and 350 °C (the lowest temperature to synthesize mesoporous Cr_2O_3 crystals within SBA-15[11]), respectively. To reveal the limitation of the solid−liquid method, crystal growth of PbO, which decomposes at a low temperature (>205 °C) without melting, was tested. $(NH_4)_2Cr_2O_7$, which decomposes at 180 °C without melting, was also selected as a precursor for further confirmation of the mechanism.

Specimens were characterized using X-ray powder diffraction (XRD) on a Philips reflective diffractometer with Cu Kα radiation (λ = 0.1542 nm) and high-resolution transmission electron microscopy (HRTEM) on a JEOL JEM-2011 electron microscope operated at 200 kV. TEM images were recorded with a Gatan 794 CCD camera. Energy-dispersive X-ray microanalysis (EDX) was performed to qualitatively detect the elements present. Selected area electron diffraction (SAED) was used to determine the crystallinity of the materials and to identify the crystallographic systems. The powder specimen was finely ground and pressed onto a sample holder for XRD examination. For TEM examination, the powder specimen was ground in acetone and 1 drop of the suspension was deposited on a copper specimen grid with a holey carbon film.

Table 1. Melting Points and Decomposition Temperatures of the Precursors for Porous Transition Metal Oxides

precursor	melting point	decomposition	oxide product
$Ce(NO_3)_3{\cdot}6H_2O$	96 °C	200 °C	CeO_2
$Cr(NO_3)_3{\cdot}9H_2O$	66 °C	>100 °C	Cr_2O_3 (>350 °C)
$Co(NO_3)_2{\cdot}6H_2O$	55 °C	>74 °C	Co_3O_4 (>150 °C)
$Ni(NO_3)_2{\cdot}6H_2O$	56.7 °C	>110 °C	NiO
$Pb(NO_3)_2$		205−223 °C	PbO
$(NH_4)_2Cr_2O_7$		180 °C	Cr_2O_3 (>180 °C)

3. Results and Discussion

Transition metal nitrates, $Co(NO_3)_2{\cdot}6H_2O$, $Ni(NO_3)_2{\cdot}6H_2O$, $Ce(NO_3)_3{\cdot}6H_2O$, and $Cr(NO_3)_3{\cdot}9H_2O$, are solid at room temperature. They entered the liquid state when the temperature increased to their melting points with or without losing structural water. The metal nitrates decomposed into oxides when the temperature further increased to their decomposition temperatures (higher than their melting points for the nitrates studied in the present work), and crystal growth of oxides occurred at a higher temperature. Table 1 shows the melting points and decomposition temperatures of the nitrates in question and two other selected precursors.

It was found that the solid−liquid method worked well with these four nitrate precursors. Since the melting points of these nitrates are low, with the increase of temperature, the nitrates turned into a liquid phase before decomposition and moved into the mesopores of the template SBA-15 or KIT-6 with capillary action. The nitrates decomposed and crystallization of the corresponding oxides took place inside the mesopores at a higher temperature.

SBA-15 contains hexagonally close-packed straight mesopores connected by some smaller nanochannels and/or micropores. KIT-6 has a cubic mesostructure, consisting of a three-dimensional bicontinuous channel network. These two interlaced mesopores in KIT-6 may also be connected to each other by some small nanochannels. Therefore, we expect the negative replicas of these silica templates should have structures as shown in Figure 1.

Figure 2 shows typical TEM images of the SBA-15 templated porous crystals. The morphologies of these particles are the same, i.e., an array of nanorods connected to each other by some small bridges, which can be seen more clearly in the HRTEM images in Figure 3. Earlier HRTEM studies of the small bridges in the SBA-15 templated materials include the work by Terasaki's group[31] and Zhou and co-workers.[7] If these small channels in SBA-15 were

(24) Katou, T.; Lee, B.; Lu, D. L.; Kondo, J. N.; Hara, M.; Domen, K. *Angew. Chem., Int. Ed*. **2003**, *42*, 2382.
(25) Roggenbuck, J.; Koch, G.; Tiemann, M. *Chem. Mater*. **2006**, *18*, 4151.
(26) Li, H. F.; Zhu, S. M.; Xi, H. A.; Wang, R. D. *Microporous Mesoporous Mater*. **2006**, *89*, 196.
(27) Jacobsen, C. J. H.; Madsen, C.; Houzvicka, J.; Schmidt, I.; Carlsson, A. *J. Am. Chem. Soc*. **2000**, *122*, 7116.
(28) Wang, Y. M.; Wu, Z. Y.; Shi, L. Y.; Zhu, J. H. *Adv. Mater*. **2005**, *17*, 323.
(29) Wang, Y. M.; Wu, Z. Y.; Zhu, J. H. *J. Solid State Chem.* **2004**, *177*, 3815.
(30) Jiang, Q.; Wu, Z. Y.; Wang, Y. M.; Cao, Y.; Zhou, C. F.; Zhu, J. H. *J. Mater. Chem.* **2006**, *16*, 1536.
(31) Liu, Z.; Terasaki, O.; Ohsuna, T.; Hiraga, K.; Shin, H. J.; Ryoo, R. *ChemPhysChem* **2001**, *2*, 229.

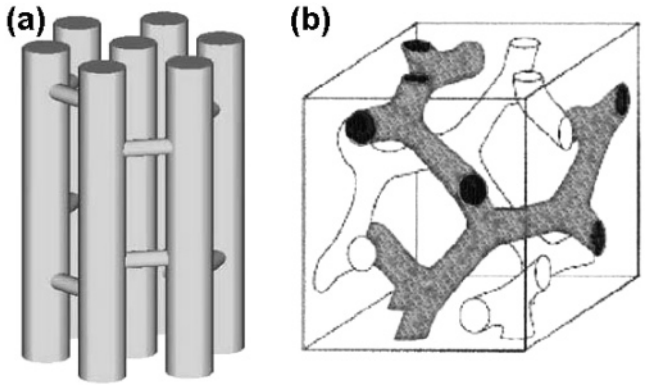

Figure 1. Schematic drawing of morphologies of porous crystals of oxides templated by (a) SBA-15 and (b) KIT-6.[4]

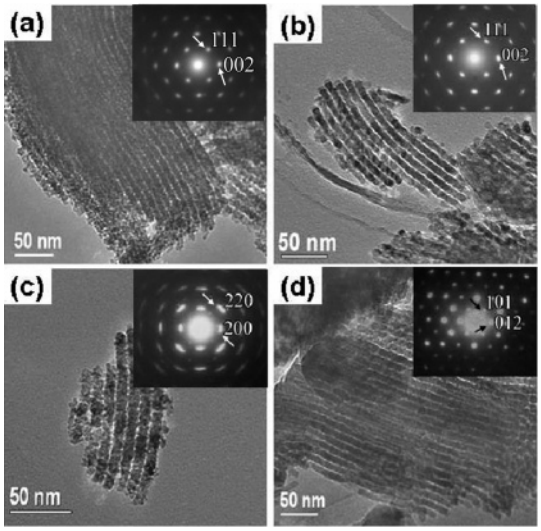

Figure 2. TEM images of SBA-15 templated porous single crystals of (a) Co_3O_4, (b) NiO, (c) CeO_2, and (d) Cr_2O_3. The insets are SAED patterns of the oxides showing single-crystal property of each specimen.

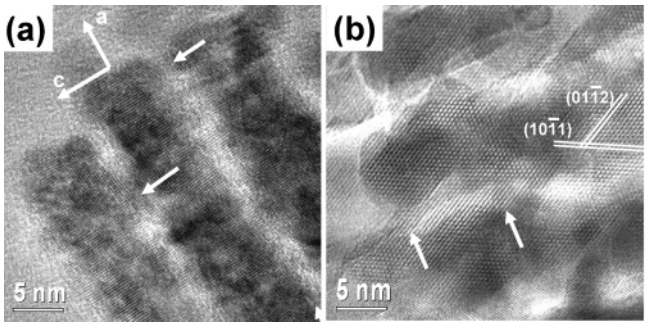

Figure 3. HRTEM images of SBA-15 templated porous single crystals of (a) CeO_2 and (b) Cr_2O_3. Some small bridges in the nanochannels connecting the nanorods are indicated by arrows.

not replicated, short nanorods would be produced instead of a three-dimensional network.[32] SAED from these particles, the selected areas normally covering the whole particle or at least several nanorods, show typical single-crystal patterns as seen in the insets of Figure 2. In detail, the SAED pattern in Figure 2a can be indexed onto the face-centered cubic (fcc) unit cell of Co_3O_4, space group $Fd\bar{3}m$ with the cell parameter $a = 0.8085$ nm, when the view direction is along the [$\bar{1}$10] zone axis. The (002) should be systematically

(32) Zhu, K. K.; He, H. Y.; Xie, S. H.; Zhang, X.; Zhou, W. Z.; Jin, S. L.; Yue, B. *Chem. Phys. Lett.* **2003**, *377*, 317.

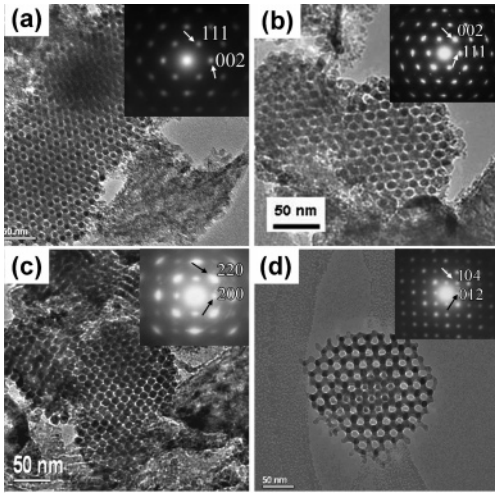

Figure 4. TEM images of porous single crystals of (a) Co_3O_4, (b) NiO, (c) CeO_2, and (d) Cr_2O_3 templated by KIT-6. The insets are SAED patterns, showing single-crystal property for each specimen and being indexed onto the corresponding oxide crystal structures.

absent according to the space group of Co_3O_4. Its appearance is due to multiple scattering. The SAED pattern in Figure 2b is indexed to the fcc unit cell of NiO with $a = 0.4176$ nm, space group $Fm\bar{3}m$. The inset in Figure 2c is a SAED pattern from fcc CeO_2 with $a = 0.54124$ nm, space group $Fm\bar{3}m$, on the [001] projection. The porous single-crystal property of rhombohedral Cr_2O_3 with $a = 0.4951$ and $c = 1.3598$ nm, space group $R\bar{3}c$, is also confirmed by SAED (inset in Figure 2d) when viewed down the [12$\bar{1}$] direction.

HRTEM images from these specimens further confirm the single-crystal property by showing that the crystal orientations from any part of a particle are the same. Figure 3 shows HRTEM images from CeO_2 and Cr_2O_3, viewed down the [010] and [121] zone axes, respectively. Some small bridges between the nanorods are also imaged. The atomic images show that the crystal orientations of all the nanorods as well as the small bridges in a particle are uniform. It can therefore be concluded that, during the crystal growth, the crystal expands from one mesopore to another through the nanochannels in SBA-15.

Similar results were obtained from the KIT-6 templated crystals as shown in Figure 4. Since the pore system in KIT-6 is three-dimensional in a cubic symmetry, spherical particles of the porous crystals of oxides were normally developed, although the crystal structures of the oxides are the same as those templated by SBA-15. The insets in Figure 4 can be indexed onto the structures of the oxides, when viewed down the [$\bar{1}$10] of Co_3O_4, [1$\bar{1}$0] of NiO, [001] of CeO_2, and [42$\bar{1}$] of Cr_2O_3 zone axes, respectively. Monocrystal property of the particles is undoubtedly proved.

Another interesting phenomenon is that the densities of porous crystals of Co_3O_4, NiO, and CeO_2 are much higher than that of Cr_2O_3, indicating that the former replicated both interlaced pores of KIT-6, while the latter only replicated one of them. This estimation was made based on the TEM image contrast patterns. When both the interlaced pores are replicated, no empty holes can be seen along the [111] direction of the mesostructure (Figures 4a and 4b). The empty holes can be observed on this projection when only one of the interlaced pores is replicated as seen in the case of Cr_2O_3

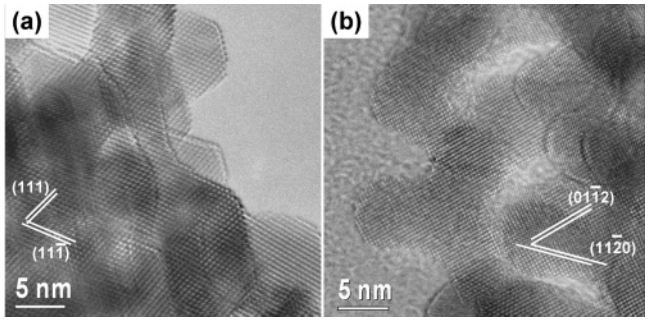

Figure 5. HRTEM images of porous single crystals of (a) Co_3O_4 and (b) Cr_2O_3 templated by KIT-6.

(Figure 4d), although a small area in the center of the particle in Figure 4d shows a replication of both pores. The TEM images on the [100] projection can also be used for this comparison. Such a difference was previously observed from KIT-6 templated porous crystals of Co_3O_4 and Cr_2O_3 using the evaporation method and was believed that the high crystallization temperature of Cr_2O_3 made small channels connecting the two interlaced pores blocked. The conclusion was supported by surface area measurements.[11]

HRTEM images further confirmed the monocrystal property of the specimens. Two examples are given in Figure 5, recorded from porous Co_3O_4 and Cr_2O_3. Because there is no specific relation between the oxide crystal orientation and the orientation of the mesopore structure, when we looked down a principal zone axis of the crystal structure, the view direction is normally not parallel to any principal orientation of the mesopore structure. Consequently, the regular mesopores cannot be observed in the HRTEM images in Figure 5. However, the pores and the nanorod sizes can still be directly seen, allowing us to measure the diameter of the nanorods, 7.6 nm (Co_3O_4), 6.9 nm (Cr_2O_3), and 6.7 nm (NiO and CeO_2). All these values are slightly smaller than the measured pore diameter in KIT-6 (~8 nm).

The specimens were also characterized by other techniques. For example, the chemical composition was examined by EDX and the monophasic state was confirmed by XRD. In comparison with previously prepared porous crystals of oxides using other methods, such as SBA-15 templated Co_3O_4,[8,9,11] Cr_2O_3,[7−9,11] CeO_2,[8,9,33] and NiO[8,9,34] and KIT-6 templated Co_3O_4,[11,12] Cr_2O_3,[10,11] and CeO_2,[31,35] the qualities of the products in the present work are at least equally good. On the other hand, the greatest advantages of the newly developed technique are its simplicity and low cost and it is solvent-free. The complicated surface functionalization, selection of limited suitable heteropolyacids, long periods of stirring or evaporation, and use of solvent can all be avoided.

To compare the evaporation method and solid−liquid method, in another set of parallel experiments, $Cr(NO_3)_3 \cdot 9H_2O$ was impregnated into SBA-15 by both methods. These two samples were heated at 70 °C (for melting), 110 °C (for decomposition), and 350 °C (for crystal growth of Cr_2O_3),

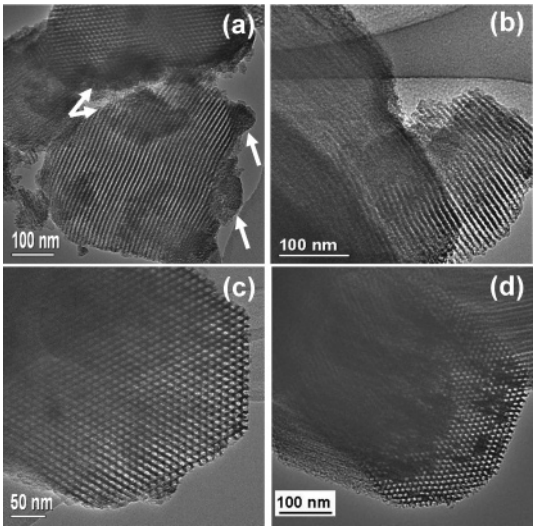

Figure 6. TEM image of the decomposition process of $Cr(NO_3)_3 \cdot 9H_2O$ toward Cr_2O_3 within SBA-15. (a) A mixture of $Cr(NO_3)_3 \cdot 9H_2O$ and SBA-15 using the solid−liquid method before calcination. (b) Specimen prepared in the evaporation method after evaporation of ethanol before calcination. Specimen (a) was heated at 70 °C for 5 h (c), following further heating at 350 °C for 5 h (d).

respectively. Specimens at different stages were examined by TEM (Figure 6).

Before calcination, two separated phases can be observed from the specimen prepared using the solid−liquid method, SBA-15 and $Cr(NO_3)_3 \cdot 9H_2O$ (Figure 6a). Some of the latter particles are indicated by the arrows. On the other hand, only SBA-15 particles can be identified without large crystallites on their surface in the specimen before calcination prepared using the evaporation method (Figure 6b). It is probably because $Cr(NO_3)_3 \cdot 9H_2O$ was dissolved in solvent (ethanol) and dispersed well on the outside surface of the SBA-15 particles. Since the particles were very small and the compound, containing water, was beam-sensitive, it is difficult to record HRTEM images for these small particles. However, the EDX spectra from the specimen areas without notable metal-containing particles still showed Cr peaks and O and Si peaks. The XRD patterns of the sample prepared using the solid−liquid method confirmed the presence of crystalline phase $Cr(NO_3)_3 \cdot 9H_2O$ (Figure 7a). Diffraction peaks of $Cr(NO_3)_3 \cdot 9H_2O$ (not shown) were also observed from the sample made using the evaporation method, indicating a crystalline phase with poor crystallinity.

After $Cr(NO_3)_3 \cdot 9H_2O$/SBA-15 was heated at 70 °C for 5 h, only SBA-15 particles could be observed from both samples prepared in different methods (Figure 6c). Heating at 110 °C for 5 h did not make any difference in the TEM appearance. XRD did not detect any crystalline phase from the specimens after heating at 70 and 110 °C (Figures 7b and 7c). After $Cr(NO_3)_3 \cdot 9H_2O$/SBA-15 was heated at 350 °C for 5 h, the oxide partially filled the pores of SBA-15, forming individual nanoparticles, which was observed in TEM images (Figure 6d). The corresponding XRD pattern shows a crystalline phase of Cr_2O_3 (Figure 7d).

It is believed that the limitation of the solid−liquid method is that the precursor must have a melting point lower than its decomposition temperature. To further understand the mechanism of the chemical process in the solid−liquid

(33) Rossinyol, E.; Arbiol, J.; Peir'o, F.; Cornet, A.; Morante, J. R.; Tian, B.; Bo, T.; Zhao, D. *Sens. Actuators B* **2005**, *109*, 57.
(34) Wang, Y. G.; Xia, Y. Y. *Electrochim. Acta* **2006**, *51*, 3223.
(35) Shen, W. H.; Dong, X. P.; Zhu, Y. F.; Chen, H. R.; Shi, J. L. *Microporous Mesoporous Mater.* **2005**, *85*, 157.

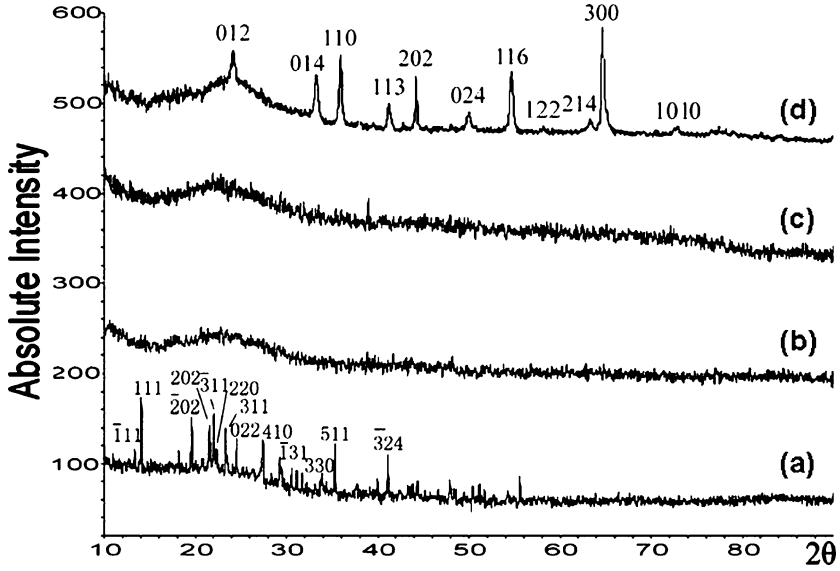

Figure 7. XRD patterns of different phases during thermal treatment of $Cr(NO_3)_3 \cdot 9H_2O$: (a) before heating, (b) at 70 °C for 5 h, (c) at 110 °C for 5 h, and (d) at 350 °C for 5 h within SBA-15. Pattern (a) is indexed onto the crystal structure of $Cr(NO_3)_3 \cdot 9H_2O$ and pattern (d) indexed to the Cr_2O_3 structure.

method, we selected $Pb(NO_3)_2$ and $(NH_4)_2Cr_2O_7$ as precursors for fabricating porous crystals of PbO and Cr_2O_3 in the SBA-15 template. $Pb(NO_3)_2$ decomposes at about 210 °C without melting and $(NH_4)_2Cr_2O_7$ decomposes at 180 °C, forming oxides outside the mesopores of SBA-15. Consequently, no porous crystals were obtained.

According to the statement in the previous report for the evaporation method, the precursor is dissolved in a solvent and can migrate into the pores when the solvent is evaporated. Both $Pb(NO_3)_2$ and $(NH_4)_2Cr_2O_7$ were also used as precursors in the evaporation method. Although the TEM images of the specimens after evaporation but before thermal treatment showed no crystallites of $Pb(NO_3)_2$ and $(NH_4)_2Cr_2O_7$, similar to that in Figure 6b, thermal treatment did not result in any porous crystals. This is the evidence to support the theory that, during the evaporation of solvent, the precursor cannot move into the mesopores of silica. Instead, the precursor more likely stays on the surface of template particles as very small crystallites and migrates into the pores only when it melts in the case of $Co(NO_3)_2 \cdot 6H_2O$, $Ni(NO_3)_2 \cdot 6H_2O$, $Ce(NO_3)_3 \cdot 6H_2O$, and $Cr(NO_3)_3 \cdot 9H_2O$. Since $Pb(NO_3)_2$ and $(NH_4)_2Cr_2O_7$ decompose without melting, crystal growths of PbO and Cr_2O_3 take place only outside the mesopores, leading to nonporous crystals.

4. Conclusion

We demonstrated a simple, solvent-free (therefore environmentally friendly), synthetic method for fabrication of porous single crystals of transition metal oxides. If a precursor has a low melting point, when it simply mixes with a silica template, it may melt before decomposition into another solid phase which normally has a higher melting point and migrates into the mesopores of silica. Decomposition and crystal growth of oxides inside the mesopores will result in porous single crystals of oxides. We have also found out that the previously proposed mechanism of impregnation of precursors into the mesopores during evaporation of solvent in the evaporation method is not correct. The difference between the evaporation method and the newly developed solid−liquid method is that the former gives a better distribution of precursor on the surface of the template particles. However, it is proved that this difference makes no significant difference in the final products of porous crystals of oxides. Consequently, the solid−liquid method described in the present work is more attractive for industry applications. We noticed that the yields of the products in the present work are still not high enough, about 70−80% (Co_3O_4), 40% (NiO and Cr_2O_3), and 20% (CeO_2), estimated from the TEM observation. Similar values were obtained from the specimens in the parallel syntheses using the evaporation method. Refinement of the synthesis conditions is being carried out for high yields in this laboratory. When better samples are produced, N_2 sorption experiments for detecting the pore properties and measurements of physicochemical properties will also be performed.

Acknowledgment. W.Z. thanks St. Andrews University for an EaSTCHEM studentship for W.Y.

CM070124B